PHYSICAL REVIEW E **71**, 046407 (2005)

Thomson scattering measurements of heat flux from ion-acoustic waves in laser-produced aluminum plasmas

Q. Z. Yu, J. Zhang,* Y. T. Li, and X. Lu
Laboratory of Optical Physics, Institute of Physics, Chinese Academy of Sciences, P. O. Box 603, Beijing 100080, China

J. Hawreliak and J. Wark
Department of Physics, Clarendon Laboratory, Oxford University, Oxford OX1 3PU, United Kingdom

D. M. Chambers
Steward Observatory, University of Arizona, Tucson, Arizona 85721, USA

Z. B. Wang and C. X. Yu
Department of Modern Physics, University of Science and Technology of China, Hefei 230026, China

X. H. Jiang, W. H. Li, S. Y. Liu, and Z. J. Zheng
Research Center for Laser Fusion, China Academy of Engineering Physics, Mianyang 621900, China

(Received 2 June 2004; revised manuscript received 27 December 2004; published 25 April 2005)

Thomson scattering (TS) measurements are performed at different locations in a laser-produced aluminum plasma. Variations of the separation, wavelength shift, and asymmetric distribution of the two ion-acoustic waves are investigated from their spectral-time-resolved TS images. Detailed information on the space-time evolution of the plasma parameters is obtained. Electron distribution and variation of the heat flux in the plasma are also obtained for a steep temperature gradient.

DOI: 10.1103/PhysRevE.71.046407 PACS number(s): 52.38.−r, 52.25.Os, 52.35.Fp, 52.50.Jm

I. INTRODUCTION

The interaction of a high-intensity laser pulse with plasma is of currently great interest, both for understanding of the interaction physics and for potential applications in x-ray lasers [1–3], inertial confinement fusion [4,5], and electron accelerators [6,7]. The success of these applications greatly depends on the efficient absorption of laser energy. Some physical processes, such as stimulated scattering instabilities, inverse bremsstrahlung (IB) absorption, and modulation and filamentation instabilities are much influenced by the properties of plasmas [8–10]. For example, the stimulated Brillouin and Raman scattering, which can greatly affect laser energy absorption, depend strongly on the gradients of the electron density and temperature. Thus it is important to develop an accurate diagnostic method for measuring the instantaneous plasma parameters. Thomson scattering provides an excellent tool to study hydrodynamic processes in a very small region of the plasma [11–15]. By irradiating the plasma with a probe laser beam, and collecting the spectra scattered by the electrons, one can obtain the time-resolved ion-acoustic image of any region and deduce the temporally hydrodynamic parameters of the plasma.

In this paper, we present the results from measurements of the ion-acoustic images from a Thomson scattering experiment. The temporally resolved spectra corresponding to three different regions in the plasma are obtained. Typical features of the two ion-acoustic peaks are analyzed. The evolution of the electron temperature and plasma expansion velocity are measured as functions of time and space. The heat flux in the plasma with steep temperature gradient is calculated using the flux-limited theory.

II. EXPERIMENTAL SETUP

The experiment was performed with the Shenguang II Nd:glass laser facility at the National Laboratory of High Power Laser, China. The schematic of the experimental setup is shown in Fig. 1(a). A 1ω (1.053 μm) heater beam was

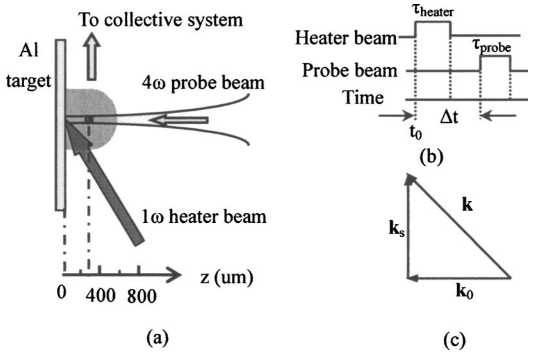

FIG. 1. (a) Schematic of the experimental setup. (b) Relative beam timings: τ_{heater} and τ_{probe} are the pulse durations of the heater and the probe beams, respectively, t_0 corresponds to the time at which the heater beam reaches the target surface, and $\Delta t = 1.7$ ns is the delay time of the probe beam relative to the heater beam. (c) The scattering diagram.

---

*Author to whom all correspondence should be addressed. Electronic address: jzhang@aphy.iphy.ac.cn

1539-3755/2005/71(4)/046407(6)/$23.00

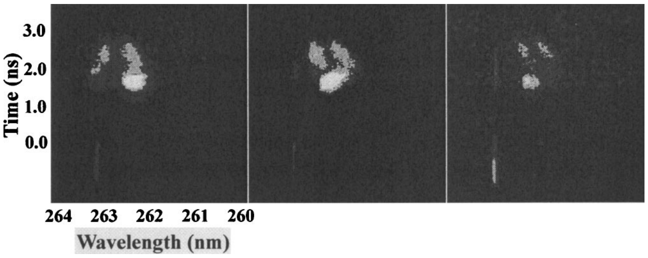

FIG. 2. Streaked Thomson scattering spectra of Al plasmas at various positions of $z=200$, 300, and 400 μm in the plasma. $\lambda_0=263.3$ nm is the wavelength of the probe laser beam.

smoothed with a random phase plate to produce a plasma by irradiating an aluminum disk at an angle of 60° to the disk normal. We used a typical laser pulse of duration 1 ns (full width at half maximum) and energy about 300 J. The focal spot size, measured by an x-ray pinhole camera, was about 200 μm in diameter, indicating a laser intensity of $I_{\text{heater}} \approx 1\times 10^{15}$ W/cm^2 on the disk.

The Thomson scattering probe laser beam was focused at different locations to probe the laser-produced plasma. In order to measure the evolution of the laser-produced plasma, the probe beam was delayed 1.7 ns relative to the heater beam, as shown in Fig. 1(b). The probe beam was perpendicular to the disk and focused to a spot with diameter about 100 μm. The probe beam was operating at 4ω ($\lambda_0=263.3$ nm) with an energy of approximately 30 J in a 1 ns Gaussian pulse, resulting in an intensity of $I_{\text{probe}}=3.8\times 10^{14}$ W/cm^2. As we will verify below, the effect of the probe beam on the plasma is small due to its low energy.

The scattered radiation was collected at a scattering angle of $\theta=90°$ with $f/3.6$ optics and 10× magnification onto the 50 μm entrance slit of an optical spectrometer with a 2400 grooves per mm grating. The cylindrical Thomson scattering volume, determined by the focal spot of the probe laser beam and the slit of the spectrometer, was 50 μm long and 100 μm in diameter. The spectrally resolved Thomson scattering signal was recorded by an optical streak camera coupled to a charge-coupled device, resulting in a spectral and temporal resolution of 0.1 nm and 10 ps, respectively. Only very weak stray light is produced by this arrangement of the probe beam and the collection shown in Fig. 1(a).

III. EXPERIMENTAL RESULTS

The spectra of the Thomson scattered (TS) radiation are related to the scattering parameter α, which determines whether the scattering is sensitive to plasma-wave fluctuations. In our experiment, $\alpha=1/(\mathbf{k}\lambda_D)>3$, $\mathbf{k}=\mathbf{k}_0-\mathbf{k}_s$, where $\mathbf{k}$, $\mathbf{k}_s$, and $\mathbf{k}_0$ are the scattering, scattered, and probe wave vectors, respectively, as defined in Fig. 1(c), and λ_D is the electron Debye length [16]. The radiation is predominantly scattered into a narrow region near the frequency of the probe beam. Figure 2 are three recorded TS images corresponding to different detecting regions of $z=200$, 300, and 400 μm away from the target surface, respectively. For $t_0+1.7<t<t_0+2.4$ ns, where t_0 denotes the beginning of the heater beam, two distinct ion-acoustic peaks of the Thomson scattering can be seen. The narrow line at the lower left corner of the image corresponds to the probe beam, which give us a fiducial wavelength of $\lambda_0=263.3$ nm. It is clearly seen that the separation of the two resonance peaks decreases with time in the three images, indicating that without the heater beam, the plasma cools down because of radiation loss and spatial expansion. The whole spectrum is apparently blueshifted from the probe beam, indicating a rapid expansion of the plasma in the scattering volume. Away from the target surface, a much larger blueshift of the two ion-acoustic peaks can be seen. Furthermore, the two satellites are nearly symmetrical at $z=400$ μm, but somewhat asymmetrical at the position 300 μm away from the target and more obvious at $z=200$ μm. This means that the critical density surface is between the positions of 300 and 400 μm from the target surface. More precisely, the position at $z=300$ μm is inside but the position at $z=400$ μm is almost outside of the critical density surface.

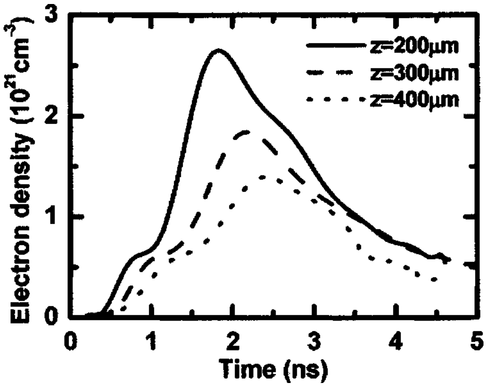

FIG. 3. Simulated temporal electron density at three different positions. $z=300$ μm is inside the critical density surface, and $z=400$ μm is outside the critical surface.

The evolution of laser-produced plasma is numerically simulated using MEDUSA, a one dimensional Lagrangian hydrodynamic code. Figure 3 shows the simulated temporal variations of the electron density at different positions of the plasma. We can see that at the position of $z=400$ μm, the electron density can reach the critical density ($n_{\text{cr}}=10^{21}$ cm^{-3}) of the heater beam after the irradiating of the heater beam. But at the positions $z=200$ and 300 μm, the electron density is much higher than the critical density during most of the time when the heater beam is on. In any case, we can see the simulation also shows that $z=400$ μm is near but $z=300$ μm is inside of the critical density surface. This is consistent with the experimental result. In reality, the plasma expands laterally due to the finite focal spot of the heater beam. Simulation shows a small difference of the electron density between plasmas produced with a planar target and with a spherical target that expands laterally [16]. This enables us to use the simulated electron density below to calculate the heat flux.

The two satellites of the ion-acoustic waves, at $\omega_{\text{probe}}\pm\omega_{\text{IAW}}$, are usually used to deduce the plasma parameters. Here, ω_{probe} and ω_{IAW} are the frequencies of the probe beam and of the ion-acoustic waves, respectively. In the reference frame of the plasma, the shift frequency ω_{IAW} of the

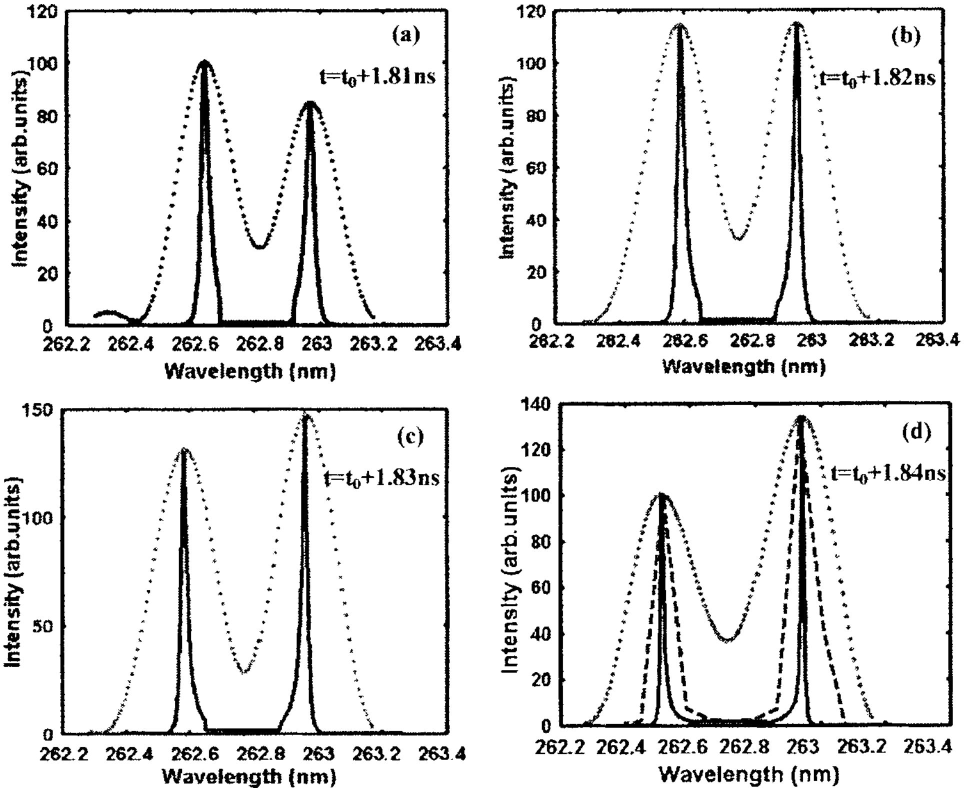

FIG. 4. Experimental (dotted line) and theoretical (solid line) spectra in arbitrary units at a distance of 300 μm from the target surface for different times (a) $t_0+1.81$, (b) $t_0+1.82$, (c) $t_0+1.83$, and (d) $t_0+1.84$ ns. The dash-dotted line in (d) corresponds to the theoretical spectrum calculated assuming an instrumental resolution of 0.1 nm.

ion-acoustic fluctuations from the central probe frequency is given by [11]

$$\left(\frac{\omega_{\text{IAW}}}{k_{ia}}\right)^2 = \frac{T_e}{M}\left(\frac{\overline{Z}}{1+k_{ia}^2\lambda_D^2} + \Gamma_i\frac{T_i}{T_e}\right) \approx \frac{T_e}{M}\left(\frac{\overline{Z}}{1+k_{ia}^2\lambda_D^2}\right), \tag{1}$$

where M is the Al ion mass, T_i the ion temperature, and Γ_i the adiabatic index, varying from 5/3 to 3.

The plasma expansion velocity is also determined by the two ion-acoustic wavelengths,

$$V = c\left(1 - \frac{\lambda_1+\lambda_2}{2\lambda_0}\right), \tag{2}$$

where λ_1 and λ_2 are the shorter and longer wavelengths of the two ion-acoustic peaks, respectively.

We have developed a numerical program based on the dynamic form factor $\mathbf{S}(\mathbf{k},\omega)$ to deduce the plasma parameters by fitting the simulation results to the experimental data. The dynamic form factor can be expressed as [17]

$$S(\mathbf{k},\omega) = \frac{2\pi}{k}\left|1-\frac{\chi_e}{\varepsilon}\right| F_e(\omega/k) + \frac{2\pi Z}{k}\left|\frac{\chi_e}{\varepsilon}\right|^2 F_i(\omega/k), \tag{3}$$

where $\varepsilon=1+\chi_e+\chi_i$ is the plasma dielectric function, $\chi_{e,i}$ are the electron (ion) susceptibilities, and $F_{e,i}$ are the one-dimensional electron (ion) velocity distribution functions in the **k** direction. Shown in Fig. 4 are the experimental and theoretical ion-acoustic features at different times, at the position 300 μm away from the target surface. To compare the ratios of the two ion-acoustic peaks, we have adjusted the experimental intensity units so that the spectrum fits the simulated one. This is possible because the positions and heights of the two peaks from the experiment and simulation fitted well. The temporal variations of the separation, the asymmetry, and the wavelength shift of the two ion-acoustic peaks are clearly shown. The parameters of the laser-produced Al plasmas, such as the electron temperature T_e the plasma expansion velocity V, the electron drift velocity U_d, and the ion-acoustic speed c_s, can also be obtained simultaneously. In the numerical program, we have assumed that the ion temperature is half of the electron temperature. The ionization degree is used as 12, as predicted by the MEDUSA hydrocode, which finds that the plasma is almost fully ionized and varies slowly with time and space. However, the width of the experimental spectrum cannot be fitted by the theoretical one. The broadened feature might be due to several reasons, such as Landau damping, plasma inhomogene-

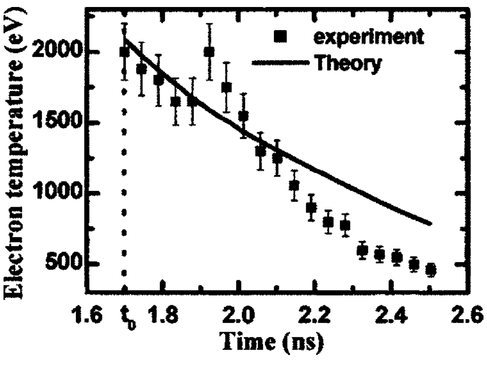

FIG. 5. Evolution of the experimental and simulated electron temperature with time, at a position 300 μm away from the target surface.

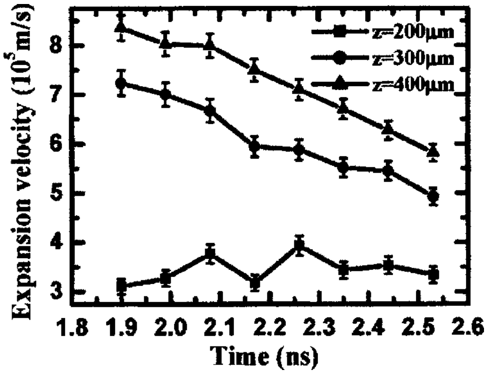

FIG. 6. Temporal development of the plasma expansion velocity at positions of 200, 300, and 400 μm away from the target surface.

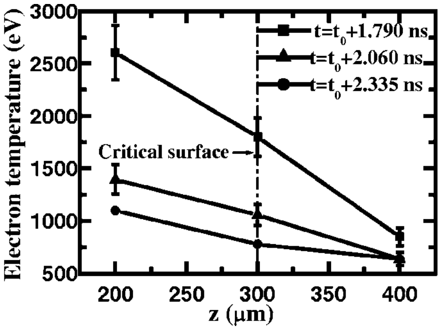

FIG. 7. Spatial variation of the electron temperature T_e at different times $t_0+1.790$, $t_0+2.060$, and $t_0+2.335$ ns.

ity, and instrumental effects. For example, Fig. 4(d) shows a theoretical spectrum with instrumental resolution of 0.1 nm. The large difference between the experimental and the broadened theoretical lines indicates that such broadening effects can be significant and must be taken into account in our experiment. Detailed investigations have been made on the broadening of the TS spectra [18,19].

IV. DISCUSSION

Temporal variations of the experimental and the simulated electron temperatures at $z=300$ μm are shown in Fig. 5. A decrease of the electron temperature with time can be observed. We can see that the electron temperature obtained experimentally agrees well with the simulated one from $t_0+1.7$ to $t_0+2.1$ ns. The deviation between the experimental and the simulated temperatures becomes larger with time. This may be due to the neglect of the dielectronic recombination in the simulation code. The vertical error bars, corresponding to the uncertainty on the location of the resonance peaks, the scattering parameter α, and the approximate of Eq. (1), are about 15% in our experiment. Another source of the error is the probe beam, which also heats the probing volume. Simulation shows the difference in the electron temperature with or without the probe beam is less than 8%.

The time evolution of the expansion velocity at different distances is shown in Fig. 6. We can see that the expansion velocity of the plasma is of the order of 10^5 m/s. At the position 400 μm away from the target surface, the expansion velocity is higher than that at 300 and 200 μm. This indicates that the plasma expands more rapidly further away from the target. On the other hand, the expansion velocity decreases with time at $z=300$ and 400 μm, and is nearly constant at $z=200$ μm. This gives us a rather clear description of the expansion process.

The spatial variations of the electron temperature at different times are presented in Fig. 7. The data are obtained from the three experimental images corresponding to the regions at $z=200$, 300, and 400 μm. The decrease of T_e from the target surface can be seen clearly. In the inner region of the plasma, the electron temperature is much higher than that of the outer region, where the electron temperature changes relatively little. The decrease of T_e at the earlier time is more rapid than that at the later time. This shows that the laser-produced plasma approaches a steady state after a rapid initial evolution. The spatial variation of the electron temperatures shows that the electron temperature gradient, which cause heat flow in the plasma, is different during the measurements.

Typical ratios of the electron-ion mean free path λ_{ei} to the temperature scale length L_T are 4.4×10^{-3}, 1.1×10^{-3}, and 5.9×10^{-4} for the times $t_0+0.09$, $t_0+0.36$, and $t_0+0.635$ ns, respectively, where $\lambda_{ei}=T_e^2/[4\pi n_e(Z+1)e^4 \ln \Lambda]$ and $L_T=T_e/(dT_e/dz)$. Because the classical thermal conductivity theory [Spitzer-Harm (SH) model] is only valid in the range of $\lambda_{ei}/L_T\leqslant 2\times10^{-3}$, our experiment is therefore at the limit of its validity. It is currently accepted that the heat flux cannot exceed a small fraction (typically 0.03) of the so-called

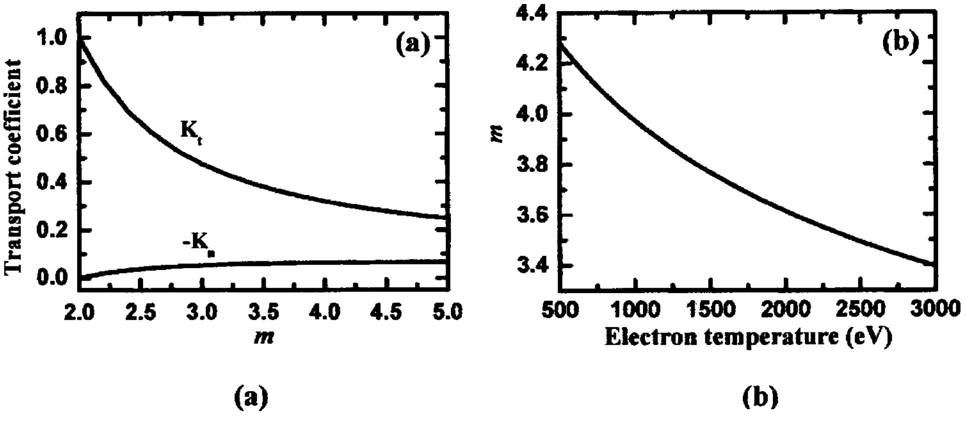

FIG. 8. (a) Variation of the exponent m with the electron temperature T_e. (b) Transport coefficients K_t and $-K_n$ as a function of the exponent m from 2 to 5.

free streaming value $q_{fs}=n_e m_e v_e{}^3$ even with Maxwellian electron distribution. Here, $v_e=(T_e/m_e)^{1/2}$ is the thermal velocity. Actually, deformation of the electron distributions always exists if the electron-electron (*e-e*) collisions are not rapid enough to Maxwellize the flat-topped electron distribution. Langdon predicted that super-Gaussian distributions would be produced in plasmas if the IB heating can compete with the *e-e* collisions [20]. According to the estimate given by Matte *et al.* [21], for high-*Z* plasmas, the electron velocity distribution can be described by a super-Gaussian distribution $f_{e0} \propto \exp[-(v/v_e)^m]$, with the index $2 < m \leqslant 5$, even when the laser energy is moderate. Clearly if there is sufficient time for *e-e* collisions, the electron distribution will be Maxwellian ($m=2$). Some detailed investigation has been made to study the electron distribution and its influence on laser energy absorption [21]. Since the super-Gaussian electron distribution leads to a crucial reduction of the heat flux, the electron distribution function should be first determined. However, so far it has not been measured experimentally because of difficulties in the diagnostics. Here we use the theory of Matte *et al.* to deduce the exponent *m*, and then to calculate the heat flux *q* with the flux-limited theory. The relationship can be written as

$$m(\sigma) = 2 + 3/(1 + 1.66/\sigma^{0.724}), \tag{4}$$

where the Langdon parameter σ is given by

$$\sigma = 0.042 \frac{I_0(\mathrm{W\ cm^{-2}})}{10^{14}} \frac{\lambda^2(\mu\mathrm{m}^2)}{1.06^2} \frac{1}{T_e(\mathrm{keV})} \overline{Z}, \tag{5}$$

where I_0 and λ are the intensity and wavelength of the heater beam, in units of W/cm and μm, respectively. Figure 8(a) shows *m* as a function of T_e. We can see that $m > 3$ in our experiment. That is, the electron distribution is much deformed due to IB absorption. The heat flux is then given by [22]

$$q = (K_t \lambda_e / L_t + K_n \lambda_e / L_n) q_f, \tag{6}$$

where $K_t = a(7b-5c)$, $K_n = 2a(b-c)$, $a = [\Gamma(3/m)]^{5/2}[3/\Gamma(5/m)]^{7/2}$, $b = \Gamma(10/m)/12$, and $c = [\Gamma(8/m)]^2/[9\Gamma(6/m)]$. Compared with that from the Maxwellian distribution, i.e., $m=2$, the transport coefficient of K_t decreases rapidly with increasing exponent *m*, although K_n remains near constant, as seen from Fig. 8(b). That is, the heat flux for a non-Maxwellian electron distribution is greatly reduced. We assume here that the density scale length is nearly equal to that of the electron temperature, i.e., $L_n \approx -L_t$. Figure 9 shows the spatial variation of the heat flux at different times. The error bars are related to the uncertainties in the exponent *m*, the ratios of λ_{ei}/L_t and λ_{ei}/L_n, the experimental electron temperature T_e, and the simulated electron density n_e. We can see that the measurement of the heat flux at $t_0 + 1.790$ ns is of the order 10^{13} W/cm^2, and it decreases rapidly away from the target surface. In the period between $t_0 + 2.060$ and $t_0 + 2.335$ ns, the heat flux is of the order 10^{12} W/cm^2, much lower than that at $t_0 + 1.790$ ns. This shows that the heat flux produced by the temperature gradient in laser-produced plasmas is very obvious in the inner regions and at the beginning of the probing time. The heat flux decreases rapidly with time, indicating that the plasma tends to be in equilibrium at the end of its evolution.

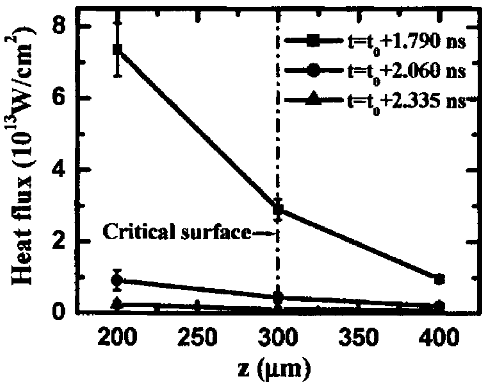

FIG. 9. Spatial variation of the heat flux at different times $t_0 + 1.790$, $t_0 + 2.060$, and $t_0 + 2.335$ ns, respectively.

V. SUMMARY

A Thomson scattering experiment was performed under and above the critical density surface in laser-produced aluminum plasmas. Temporally resolved spectra, containing much information of the plasma, are obtained at different positions in the plasma. Temporal and spatial evolution of the electron temperature T_e and the expansion velocity *V* are obtained. Electron distribution and variation of the heat flux in the plasma are also deduced under the conditions of steep temperature gradients.

ACKNOWLEDGMENTS

The authors would like to thank the staff of the Shenguang II Laser Facility at the National Laboratory of High Power Laser. This work was supported by the National Natural Science Foundation of China under Grants No. 10176034 and No. 10390160, the National Hi-tech ICF Program of China, and the National Key Basic Research Special Foundation of China under Grant No. G199075206.

---

[1] D. Umstadter, Phys. Plasmas **8**, 1774 (2001).

[2] R. Tommasini, K. Eidmann, T. Kawachi, and E. E. Fill, Phys. Rev. E **69**, 066404 (2004).

[3] S. Kiselev, A. Pukhov, and I. Kostyukov, Phys. Rev. Lett. **93**, 135004 (2004).

[4] S. H. Glenzer, C. A. Back, L. J. Suter, M. A. Blain, O. L. Landen, J. D. Lindl, B. J. MacGowan, G. F. Stone, R. E. Turner, and B. H. Wilde, Phys. Rev. Lett. **79**, 1277 (1997).

[5] C. K. Li, F. H. Séguin, J. A. Frenje, R. D. Petrasso, J. A. Delettrez, P. W. Mckenty, T. C. Sangster, R. L. Keck, J. M.

Sources, F. J. Marshall, D. D. Meyerhofer, V. N. Goncharov, J. P. Knauer, P. B. Radha, S. P. Regan, and W. Seka, Phys. Rev. Lett. **92**, 205001 (2004).

[6] V. Malka, S. Fritzler, E. Lefebvre, M.-M. Aleonard, F. Burgy, J.-P. Chambaret, J.-F. Chemin, K. Krushelnick, G. Malka, S. P. D. Mangles, Z. Najmudin, M. Pittman, J.-P. Rousseau, J.-N. Scheurer, B. Walton, and A. E. Dangort, Science **298**, 1596 (2002).

[7] S. Ya. Tochitsky, R. Narang, C. V. Filip, P. Musumeci, C. E. Clayton, R. B. Yoder, K. A. Marsh, J. B. Rosenzweig, C. Pellegrini, and C. Joshi, Phys. Rev. Lett. **92**, 095004 (2004).

[8] S. Skupin, L. Bergé, U. Peschel, and F. Lederer, Phys. Rev. Lett. **93**, 023901 (2004).

[9] A. V. Brantov, V. Yu. Bychenkov, and W. Rozmus, Phys. Plasmas **8**, 3558 (2001).

[10] J. Faure, V. Malka, F. Amiranoff, Phys. Rev. E **64**, 026404 (2001).

[11] B. Bai, J. Zheng, W. D. Liu, C. X. Yu, X. H. Jiang, X. D. Yuan, W. H. Li, and Z. J. Zheng, Phys. Plasmas **8**, 4144 (2001).

[12] D. H. Froula, L. Divol, and S. H. Glenzer, Phys. Rev. Lett. **88**, 105003 (2002).

[13] F. Amiranoff, S. D. Baton, S. Hüller, V. Malka, A. Modena, Ph. Mounaix, N. Renard-Le Galloudec, C. Rousseaux, and M. Salvati, Phys. Rev. E **61**, 1949 (2000).

[14] V. Malka, E. De Wispelaere, Ph. Mounaix, S. Hüller, F. Amiranoff, F. Dorchies, and A. Modena, Phys. Plasmas **10**, 495 (2003).

[15] J. D. Moody, E. A. Williams, S. H. Glenzer, P. E. Young, J. Hawreliak, A. Gouveia, and J. S. Wark, Phys. Rev. Lett. **90**, 245001 (2003).

[16] D. M. Chamber, S. H. Glenzer, J. Hawreliak, E. Wolfrum, A. Gouveia, R. W. Lee, R. S. Margoribanks, O. Renner, P. Sondhauss, S. Topping, P. E. Young, P. A. Pinto, and J. S. Wark, J. Quant. Spectrosc. Radiat. Transf. **71**, 237 (2001).

[17] J. Sheffield, *Plasma Scattering of Electromagnetic Radiation* (Academic, New York, 1975).

[18] J. Zheng, C. X. Yu, and Z. J. Zheng, Phys. Plasmas **4**, 2736 (1997).

[19] T. E. Tierney IV, D. S. Montgomery, J. F. Benage, Jr., F. J. Wysocki, and M. S. Murillo, J. Phys. A **36**, 5981 (2003).

[20] A. Bruce Langdon, Phys. Rev. Lett. **44**, 575 (1980).

[21] J. P. Matte, M. Lamoureux, C. Moller, R. Y. Yin, J. Delettrez, J. Virmont, and T. W. Johnston, Plasma Phys. Controlled Fusion **30**, 1665 (1988).

[22] P. Mora and H. Yahi, Phys. Rev. A **26**, 2259 (1982).